Endovenous laser coagulation: asymmetrical heat transfer (modeling in water)

Vladimir P. Minaev, Nikita V. Minaev, Vadim Yu. Bogachev, Konstantin A. Kaperiz & Vladimir I. Yusupov

ONLINE FIRST

🐴 Springer

Springer

ORIGINAL ARTICLE

Endovenous laser coagulation: asymmetrical heat transfer (modeling in water)

Vladimir P. Minaev[1] · Nikita V. Minaev[2] · Vadim Yu. Bogachev[3] · Konstantin A. Kaperiz[4] ·
Vladimir I. Yusupov[2]

Abstract

The objective of this study was to describe the dynamics of water heating carried out by continuous laser radiation with wavelengths 1.47, 1.55, and 1.94 μm with different types of fibers used for endovenous laser coagulation. The study was conducted in water using high-speed surveying of the heating process through the shadow optical method. It has been shown that in the case of highly water-absorbed laser radiations, convection and boiling play a major role in the process of heat transfer. It has been shown that in the case of radiation with $\lambda = 1.94$ μm that is heavily absorbed by water, effective heat transfer begins at significantly lower levels of power compared to the weaker-absorbed radiations with $\lambda = 1.47$ and 1.55 μm. Mathematical models based only on thermal conductivity inadequately describe the process of real heat transfer during endovenous laser coagulation. It has been established that heat transfer is sharply asymmetrical and is directed mainly up-and-forward (bare-tip fiber) or upward ("radial" and "two-ring" fibers). Heat transfer for laser light with wavelength 1.94 μm is most effective than for 1.47 and 1.55 μm.

Keywords Bare-tip · "Radial" and "two-ring" fibers · "Water-absorbing" range · Convection · Explosive boiling · EVLT · EVLA

Introduction

Over the past two decades, endovenous laser treatment (EVLT) has been widely used for the treatment of varicose veins. It is also called endovenous laser photocoagulation (EVLP) or endovenous laser ablation (EVLA). Moreover, the authors consider the most commonly used term EVLA not quite appropriate, because laser ablation implies mainly the thermal removal of a substance under the influence of laser radiation. The advantages of the EVLT method are high efficiency, low invasiveness, pain, and possibility of postoperative complications. This method is implemented using laser radiation with different wavelengths from 0.45 to 1.94 μm [1–5].

EVLT originally used optical fibers with radiation output through the fiber end (bare-tip fiber) that still remain in phlebologists' arsenal. The advantages of such fibers are their low cost and multiple use after sterilization. Since the main mechanism that triggers EVLT fibrous transformation is the thermal damage to the endothelium of the vein walls [6], more complex fibers have been introduced in which radiation is emitted as one or two rings roughly perpendicular to the fiber axis over 360°. These fibers are called "radial" and "two-ring."

A schematic image of the radiation output from different types of fibers used for EVLT is presented in Fig. 1a. The questions of the optimal wavelength, radiation power, and type of fibers for treatment are being currently discussed [7–15].

EVLT optimization requires an understanding of the processes that occur during laser exposure. The issues of mathematical and physical modeling remain relevant at the moment [9–14, 16]. Heat transfer is also an important aspect. Currently, the most popular opinion is that the main role in heat transfer is played by boiling water at the place, where radiation is emitted from the fiber, causing heat damage to

✉ Nikita V. Minaev
   minaevn@gmail.com

1   NTO IRE-Polus, pl. Akad. Vvedenskogo 1, stroenie 3,
    Fryazino, Moscow Region 141190, Russia

2   Institute of Photon Technologies, Federal Scientific Research Centre
    "Crystallography and Photonics", Russian Academy of Sciences,
    Pionerskaya ul. 2, Moscow Troitsk 108840, Russia

3   Pirogov Russian National Research Medical University,
    Ostrovityanova str.1, Moscow 117997, Russia

4   "The First Phlebological Center", Dmitriya Ul'yanova 31,
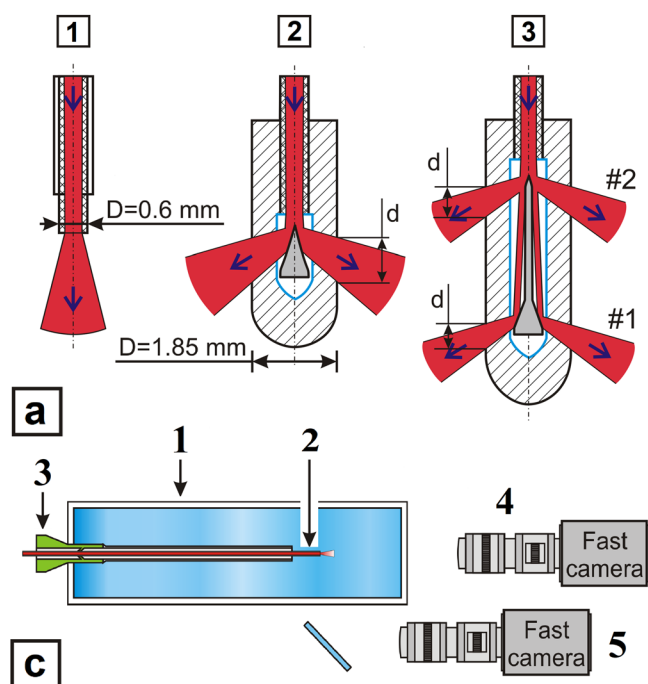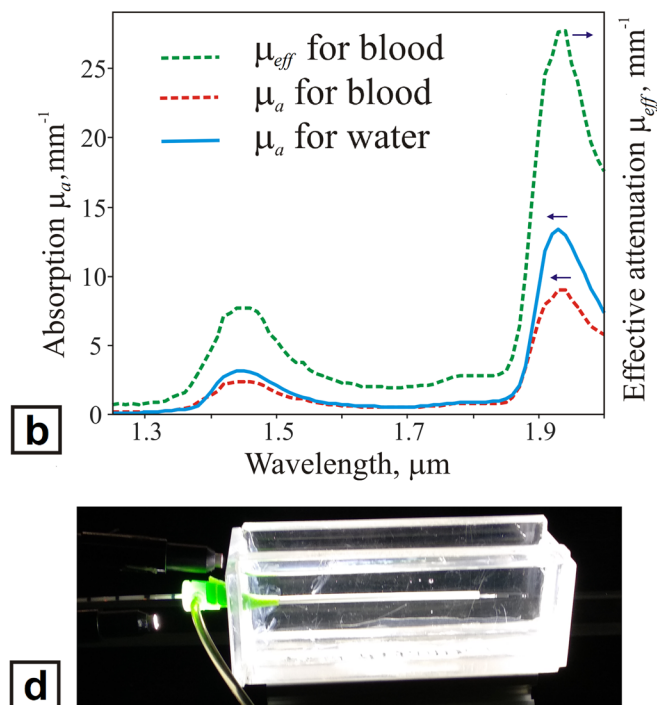   Moscow 117447, Russia

Fig. 1 (a) A schematic image of the laser radiation output from different types of fibers: 1, bare-tip; 2, "radial"; and 3, "two-ring." D, the diameter of the protective flask of the "radial" fibers. d, the width of the radiation-emitting ring. The numbers of radiation rings are marked #1 and #2. The arrows indicate the direction of laser radiation. (b) Spectral dependencies of the absorption coefficient μ_a and effective attenuation coefficient μ_{eff} in the emulsion of red blood cells (blood model with hematocrit Hct = 33.2), as well as the absorption coefficient μ_a in water. (c) Installation scheme: 1, cuvette; 2, fiber; and 3, introducer. For surveying along the axis of the fiber, a high-speed camera was installed according to scheme 4 and, for side-on surveying, according to scheme 5 with an additional mirror. (d) Picture of the cuvette with a fiber

the vein wall [6, 17]. This thesis is usually confirmed by sonograms from ultrasound devices, but they are not informative enough and allow different interpretations [16].

One should note that when the absorption of laser radiation in water prevails over absorption in hemoglobin (so-called "water-absorbing" range), the laser-induced hydrodynamic and thermal processes in the blood can be adequately modeled through processes in water. In this case, highly informative optical methods can be used to register such processes.

This paper is a continuation of the experimental studies presented in [18] and complements them by results obtained for 1.47 μm wavelength radiation and "two-ring" fibers which are also widely used or endovenous laser coagulation. As a result, the paper gives a complete picture of thermal processes realized when using the most popular for EVLK radiation wavelengths in the water-absorbing range of 1.55, 1.47, and 1.94 microns and all types of light guides used in clinical practice of EVLK: bare-tip, "radial," and "two-ring." This creates the foundation for a meaningful choice of fiber types and laser parameters.

Materials and methods

The effective depth at which laser radiation is absorbed in the blood during EVLT is determined by the effective attenuation coefficient μ_{eff}, which takes into account both absorption and scattering of radiation in the blood. In the case of water with no scattering effect, this depth is determined only by the absorption coefficient μ_a.

Figure 1 b presents the dependence of absorption coefficients for water and blood μ_a, as well as the effective attenuation coefficient μ_{eff} for the blood [19]. The characteristic thickness of the layers of water and blood, in which a significant (~ 63%) amount of laser radiation is absorbed, can be estimated accordingly by $h = 1/\mu_a$ and $h = 1/\mu_{eff}$. It should be noted that this assessment is true in the absence of the "Moses effect" [20], when super-intense boiling near the radiation output from the fiber causes the formation of a vapor gas bubble, the content of which almost does not absorb laser radiation. Table 1 contains the evaluation of the effective thickness of the layers of water and blood, in which most of the absorbed laser radiation energy transforms into heat.

Laser radiation with wavelengths from the water-absorbing range λ = 1.47, 1.55, and 1.94 μm allows for the experimental

Table 1 Effective thickness of the layers of water and blood, where laser radiation energy is absorbed

Effective thickness	λ = 1.55 μm	λ = 1.47 μm	λ = 1.94 μm
h, mm for water	1.0 ± 0.2	0.35 ± 0.07	0.08 ± 0.02
h, mm for blood	0.30 ± 0.06	0.14 ± 0.03	0.036 ± 0.007

simulation of laser-induced hydrodynamic processes in water. These processes occur in the blood before the coagulation of its organic component. This allows the use of high-speed registration of heating processes by the shadow optical method. In this method, photoregistration of light, passed through the transparent medium and detecting non-uniformity of the refractive index, caused in our case by its non-uniform heating, is carried out.

Laser devices LSP "IRE-Polyus" ($\lambda = 1.55$ μm, maximum radiation power $P_{max} = 15$ W and $\lambda = 1.94$ μm, $P_{max} = 10$ W) were used as radiation sources. The "Ceralas" device from the Biolitec company ($\lambda = 1.47$ μm, $P_{max} = 15$ W) was used in several experiments. Fibers designed for EVLT with end, "radial," and "two-ring" radiation output (Biolitec, Germany) were used. The core diameter of the fibers with end radiation output (bare-tip) was 0.6 mm. The diameter of the protective flask of the "radial" fibers was 1.85 mm. A 6F introducer (Balton, Poland) was used for putting the fibers into the water-filled cuvette (Fig. 1c, d) with dimensions $20 \times 30 \times 120$ mm^3. All experiments were made at room temperature 22–24 °C.

Images were obtained using a camera installed in two variants (Fig. 1c): for a full-face image, along the axis of the fibers, and for a side-on image, perpendicularly to the axis of the fibers with an additional mirror. Surveying was carried out using background illumination and a Fastcam SA3 high-speed camera (Photron, USA) at 4000 fps, frame duration 20 μs.

Experimental results

Radiation output through the fiber end

Figure 2 shows the high-speed frames of shady images of heat transfer in water when heated by radiation $\lambda = 1.55$ μm at $P = 12$ W. Time intervals between the frames in the picture vary depending on the process speed.

One can see in the picture that after about 50 ms after radiation switch on, a contrast structure is formed near the end of the fiber at the contact surface between the water heated by laser radiation and the cold water along the extension of the sidewall of the fiber. Its formation is caused by the appearance of a gradient of the refraction index determined by uneven changes in water temperature. This structure gradually expands upward-forward, which indicates the beginning of convective heat transfer from water heated by the absorbed laser radiation. After that, a stationary laminar transfer of heat in the upward-forward direction is formed. The speed of the heat wave front in the vertical direction is about 20 mm/s. There is no downward heat transfer.

However, along with convective heat transmission, a stable 0.1–0.2-mm-thick area with rising temperature is formed near the bottom of the fiber end. After about 0.8 s from the radiation is switched on, explosive boiling occurs near the end, resulting in the formation and subsequent collapsing of a bubble with a maximum diameter of near 5 mm (macrobubble) consisting of steam and gas that was previously dissolved in water. The formation and collapsing of the macrobubble take about 1 ms. Collapsing occurs with the formation of many vapor gas microbubbles giving heat to water during vapor condensation. Collapsing causes the formation of turbulent streams spreading heat in all directions.

There is no explosive boiling at lower levels of laser radiation power, in particular, at $P = 5$ W, and a stationary convective heat transfer process is established.

After the macrobubble collapses (frame 825 + 31.5 ms), a relatively stationary (long-lived) vapor gas bubble with sharp boundaries is formed at the fiber end. Its diameter grows to a magnitude slightly larger than the diameter of the fiber (0.6 mm). Because of the "Moses effect" [20], the radiation freely passes through the bubble and is absorbed into the water layer on its distal border. Heating results in a convective flow spreading upward-forward, as evidenced by the appearance of thermal front pictures on the frame corresponding to 950 and 975 ms.

It should be noted that the transition from convective heat transfer to bubble boiling can occur without explosive boiling [18].

Thus, the presented results show that, except for the case associated with the collapse of the vapor gas macrobubble resulting from quick (about 1 ms) explosive boiling, there is no significant downward heat transfer. It means that heat transfer occurs up and forward most of the time.

When using radiation $\lambda = 1.94$ μm, the hydrodynamic processes that determine heat transmission are manifested at significantly lower power levels compared to radiation $\lambda = 1.55$ μm due to the stronger absorption of radiation in water (Fig. 1b, Table 1).

Figure 3 presents high-speed frames of the shadow pattern of heat transfer in water when heated by radiation $\lambda = 1.94$ μm with $P = 1$ W.

In the first two frames, the appearance of the area with a refraction index gradient indicates that the heat is released at the output end of the fiber in a thin 0.2-mm layer. The speed of convective flows is low due to proximity to the fiber end. They do not have enough time for development, and therefore, the thermal fronts are not visible. At the same time, explosive boiling with the formation of a vapor gas macrobubble with a diameter of about 2 mm occurs at a power of 1 W after 38 ms after the radiation on at the fiber end. Its expansion speed is about 4 m/s. Then the macrobubble collapses after about 0.25 ms with the emission of a "cloud" of microbubbles in the forward direction and streams of heated water in all directions. Then, a pulsating vapor gas bubble with sharp borders starts to grow at the output end of the fiber (frame 44 ms). The
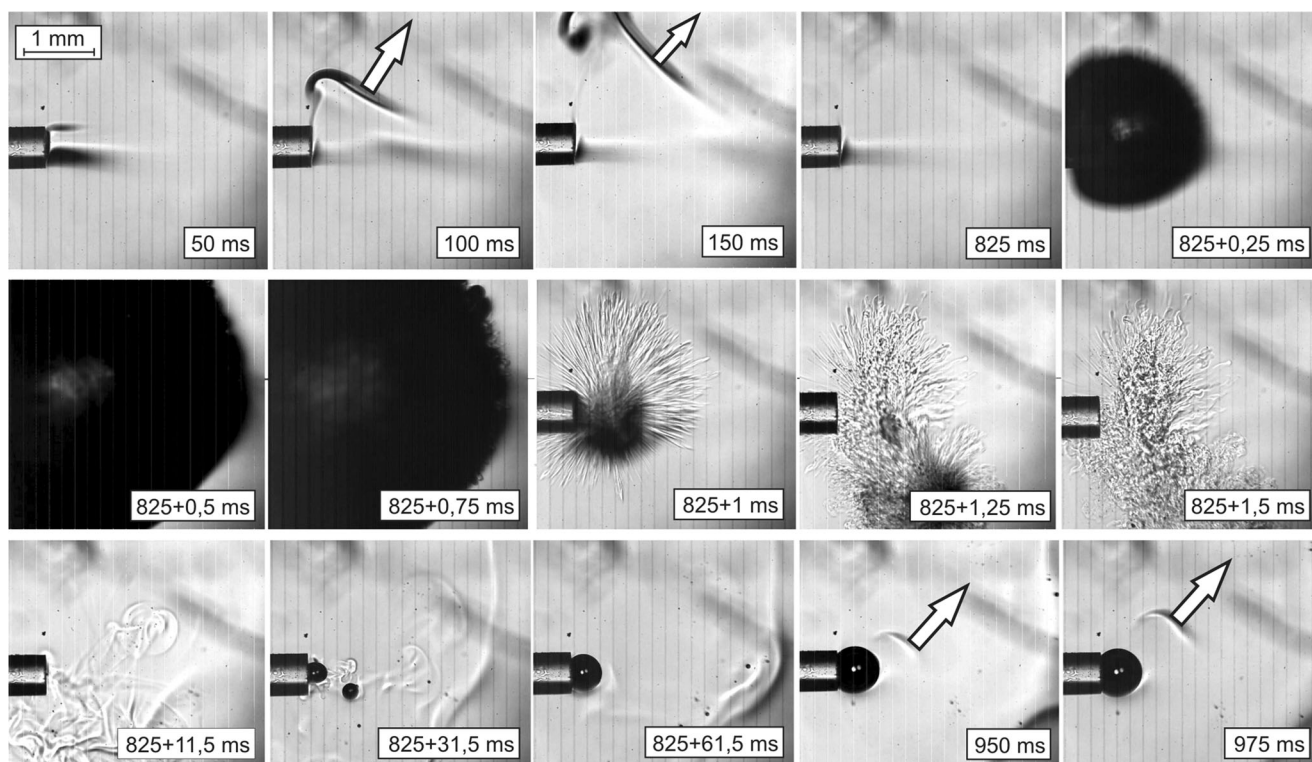
Fig. 2 Dynamics of heat transfer in water when heated by laser radiation $\lambda = 1.55$ μm, $P = 12$ W. Numbers in the frames indicate time elapsed from the radiation switching on. The arrows mark thermal fronts and the main direction of their movement

size of this bubble reaches the diameter of the fiber. As can be seen from frame 600 ms, a convective heat flow directed upward comes from the bubble top. The shadow patterns do not detect heat flows directed downward.

At power $P = 3$ W, one can observe the formation and collapsing of four steam-gas macrobubbles with a diameter of 1.5–2 mm (at 7.5, 65, 210, and 280 ms) within 0.3 s.

Thus, a pulsating bubble with sharp borders and a diameter close to the fiber diameter exists most of the time near the fiber end. With this geometry, part of the laser radiation heats wall of the bubble near the fiber, while the other part passes through the bubble and heats its distal wall. Before the formation of the next macrobubble, the pulsating bubble breaks off, and the over-heated layer of water remains near the fiber end. When the macrobubble collapses, part of it breaks off and
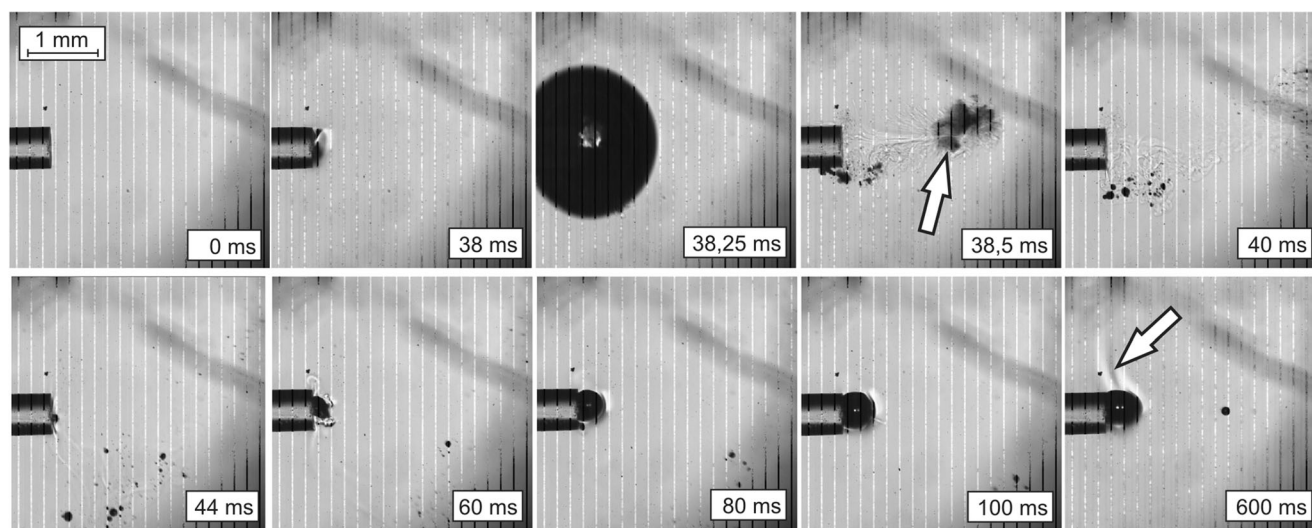

Fig. 3 Heat transfer dynamics in water when heated by laser radiation $\lambda = 1.94$ μm with $P = 1$ W. The arrow marks "microbubble cloud" (38.5 ms frame) and convective flow (600 ms frame). Numbers in the frames indicate time elapsed from switching on of the radiation

moves forward, transforming into a cloud of microbubbles, and further into turbulent flows of heated water. Boiling in the form of formation and collapsing of bubbles with a diameter of less than 0.3 mm is observed during approximately 3 ms after collapsing of the macrobubble. A long-lived pulsating bubble with a diameter of about 1 mm is re-formed after another 10 ms. Heat flows up from this bubble exists until the next explosive boiling act with the formation and collapsing of the macrobubble.

Fiber with radial radiation output

Since the main mechanism that triggers EVLT-induced fibrous transformation is the thermal damage to the vein wall, "radial" fibers (Fig. 1a) have been proposed for the procedure. In this case, radiation is emitted as a ring approximately perpendicular to the fiber axis. It was initially assumed that this made it possible to evenly affect the vein wall throughout the circumference. Experimental heating of water with laser radiation using such fibers was carried out in order to confirm this assumption.

Figure 4 a presented a high-speed frame sequence of the shadow pattern of heat transfer in water when heated by radiation emitted through a "radial" fiber with $\lambda = 1.55$ μm and $P = 15$ W. Surveying was carried out perpendicular to the fiber axis (Fig. 1c, scheme 2). One can see in Fig. 4a that in the case of a "radial" fiber with power up to $P = 15$ W, the heat transfer in water occurs due to convection and is directed upward. A stable area of heated water is formed at the bottom of the fiber, the heat from which does not spread downward, but convectively flows upward, same as in the case of end radiation output. The stationary pattern of thermal transfer through convection is established after about 0.3 s.

In the case of "radial" fibers emitting radiation with wavelength $\lambda = 1.94$ μm, the processes of effective heat transfer begin at lesser power levels compared to radiation with $\lambda = 1.55$ μm and are not limited to convective thermal transfer. Figure 4 b shows "side-on" (Fig. 1c, scheme 2) high-speed frames characterizing the dynamics of heat transfer in water when heated by radiation $\lambda = 1.94$ μm with $P = 5$ W. The first three frames correspond to heat transfer due to convection in the upward direction with the speed of heat wave front between 7 and 14 mm/s. At that, a clear front of the heat wave coming upward is observed, unlike in the case of heating by radiation $\lambda = 1.55$ μm. A vapor gas bubble grows at the fiber bottom, in which explosive boiling with the formation and collapsing of a vapor gas macrobubble starts at the moment corresponding to the fourth frame (501 ms) and lasts for about 3 ms.

The resulting microbubble cloud is transformed into turbulent streams spreading in all directions and destroying laminar convection.

After explosive boiling, small-bubble boiling starts on the surface: pulsating bubbles with a diameter of near 0.2 mm and sharp borders are formed along the perimeter of the fiber at the radiation output area. Heat flows directed upward (mostly) and to the sides are formed near these bubbles. The process of small-bubble boiling is clearly visible in Fig. 5. It shows a sequence of "full-face" shadow patterns (toward the fiber) at 2-ms intervals.

Part of the bubbles breaks off from the fiber and pops up; another part of the bubbles undergoes explosive boiling after they reach a diameter of 0.5 mm, leading to their destruction and a release of heated "protuberances." Thus, small-bubble boiling prevails in stationary mode, forming heat flows directed mainly upward. There are periodic short-term acts of "explosive" boiling against this background, in which some of the thermal flows are also directed to the sides and downward.

Fiber with "two-ring" radiation output

The processes of heat transfer using "two-ring" fibers have been studied for radiation with wavelengths $\lambda = 1.47$ μm (absorption in water three times stronger than for 1.55 μm) and $\lambda = 1.94$ μm. Figure 6 a demonstrates high-speed frames of water heating with radiation $\lambda = 1.47$ μm with $P = 15$ W; the distal end of the fiber is on the left.

One can see in the picture that more radiation energy is emitted from the ring aperture near the distal end (radiation ring #1) than from the radiation ring #2. The pictures show that the heat transfer is carried out through convection directed mainly upward. A stable heated area is formed at the bottom; there is no noticeable heat transfer downward. The speed of upward heat wave fronts is approximately 17 mm/s for the first ring and about 12 mm/s for the second ring.

Figure 6 b presents high-speed frames of the heat transfer in water when heated by radiation $\lambda = 1.94$ μm with $P = 5$ W through a "two-ring" fiber. The heat transfer pattern is similar to the one that was observed at three times higher radiation power with $\lambda = 1.47$ μm (Fig. 6a). The heat transfer has been carried out through convection within registration time, and the "explosive" boiling was not observed. The speed of the upward fronts for both rings was about 10 mm/s.

As the radiation power increases, the processes of heat transfer become more complex. Figure 7 presents high-speed frames of the shadow pattern of heat transfer in water when heated by radiation $\lambda = 1.94$ μm with $P = 10$ W prior to the first explosive boiling. After radiation switching on, there is a convective heat transfer from the second radiation ring, while a steam-gas bubble forms and begins to grow at the first radiation ring near the fiber. A clear convective heat front was not observed in this spot (Fig. 7a). After about 300 ms, an act of explosive "boiling" occurs on the first radiation ring. As a result, a vapor gas macrobubble is formed and then collapses (Fig. 7b).
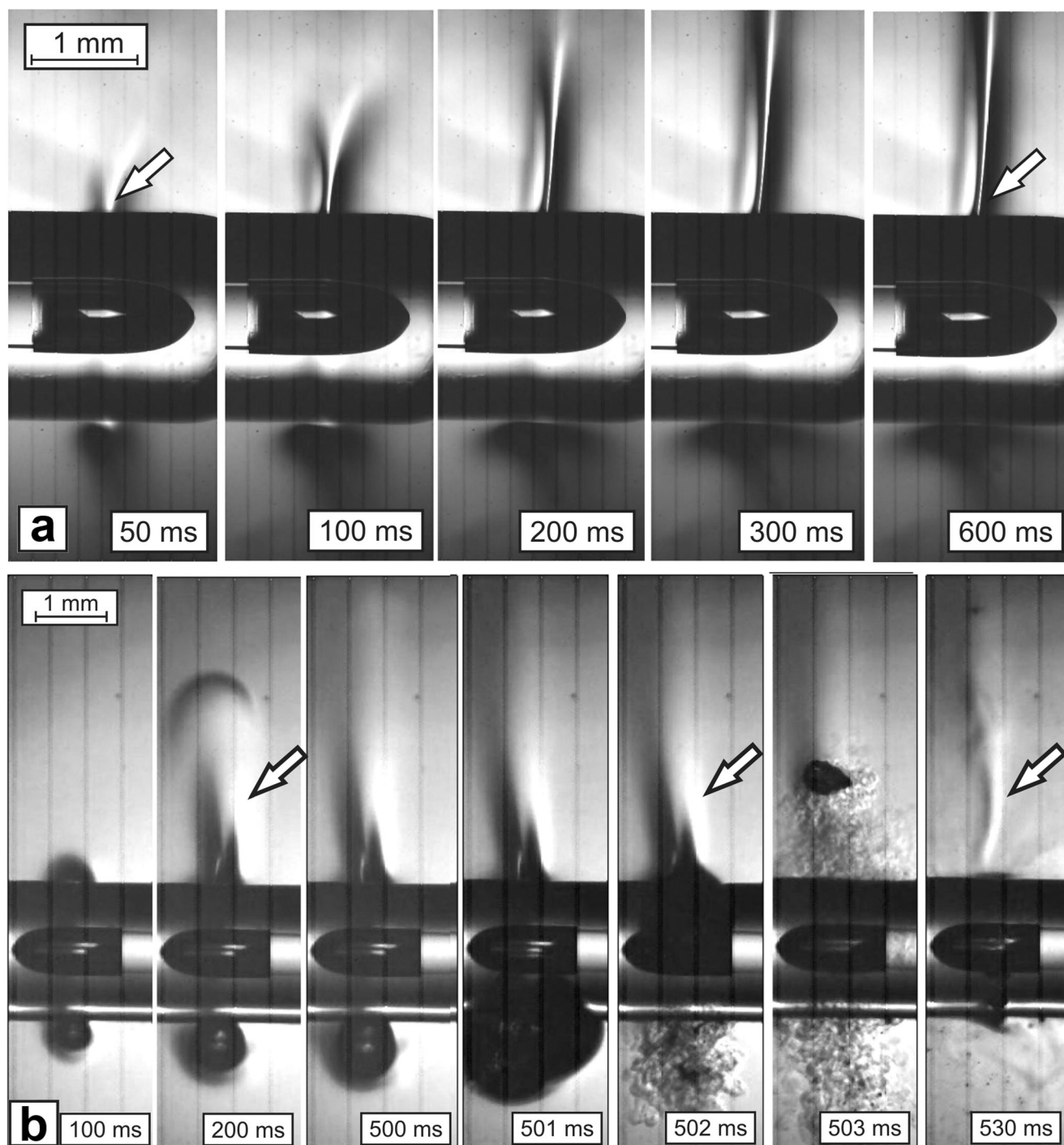
Fig. 4 Dynamics of heat transfer in water when heated by radiation (**a**) $\lambda = 1.55$ μm with $P = 15$ W and (**b**) $\lambda = 1.94$ μm with $P = 5$ W. Numbers in the frames indicate time elapsed from activation of the radiation. The arrows mark convective flows

This creates a microbubble cloud that spreads mainly upward. Microbubbles give heat to water. Then there is a pause, during which a convective flow directed upward forms at the first ring; the vapor gas bubble remains unchanged (Fig. 7b).

Then, approximately 765 ms after radiation switching on, the second act of explosive boiling occurs at the first ring with the formation and collapsing of a vapor gas bubble. It destroys

convective flow at the first radiating ring (Fig. 7c). The microbubble cloud is transformed into turbulent streams of heated water that spread in all directions. At the same time, they spread downward to a distance of no more than 2 mm.

During the entire observation period, the upward laminar convective heat transfer is carried out from the second ring,
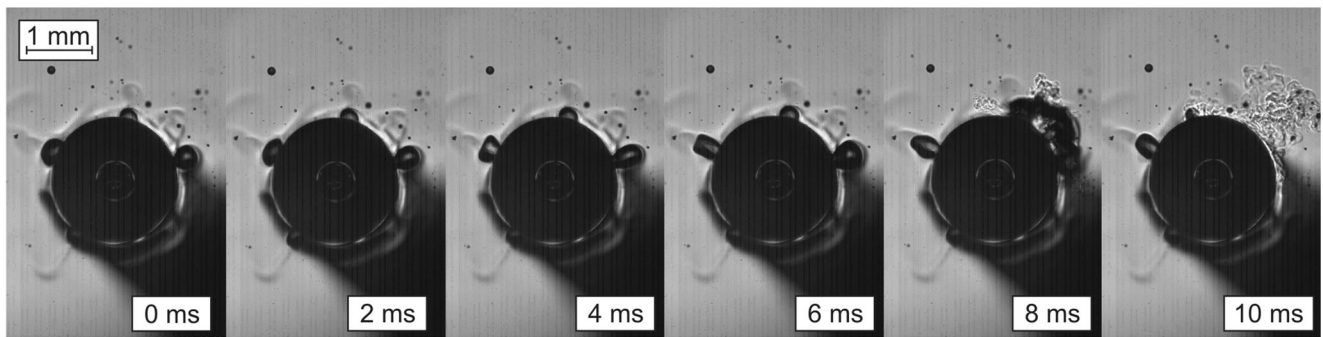
Fig. 5 Dynamics of heat transfer in water when heated by laser radiation $\lambda = 1.94\ \mu m$ with $P = 5$ W through a "radial" fiber. The stage of "small-bubble" boiling, full-face picture

through which a smaller part of radiation power is emitted. The wave front speed is about 14 mm/s.

Discussion

The advantage of using water-absorbed laser light for EVLC is based on the fact that the heating of the blood occurs mainly through water. At the same time, when the temperature reaches 100 °C, the boiling of the water begins, and the temperature does not substantially rise before evaporation, as the absorbed radiation energy is consumed to overcome the latent heat of vaporization. So, the temperature of organic blood components carbonization ≈ 250 °C is not reached (6). In this case, water in the blood boils without carbonation, providing heat transfer to the vein wall of heat necessary for its thermal damage and starting the process of fibrous substitution. Carbonation begins when organic particles (particularly those containing erythrocyte hemoglobin) are heated to a temperature of about 250 °C when they do not have time to give
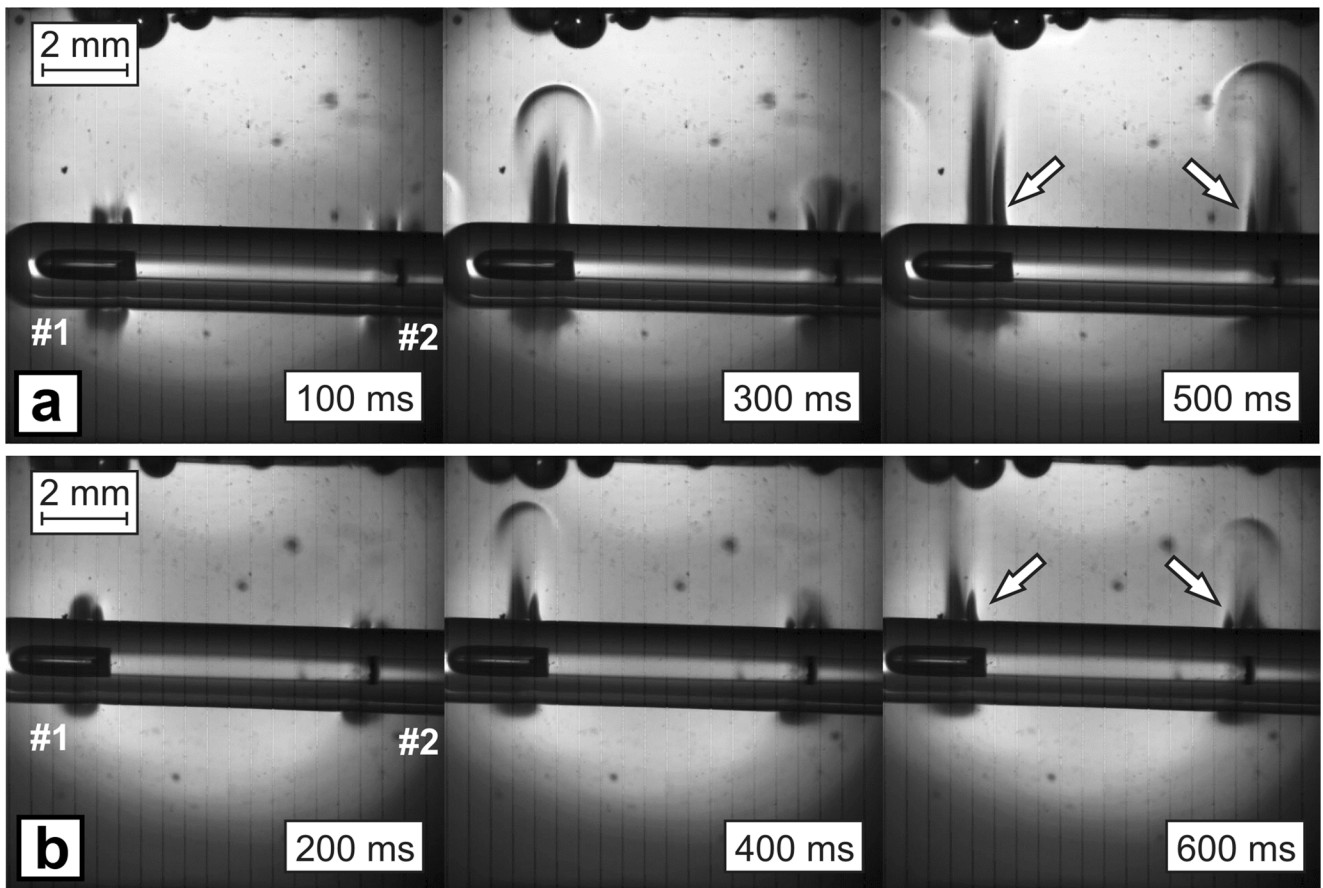

Fig. 6 Dynamics of heat transfer in water when heated by laser radiation through a "two-ring" fiber (**a**) $\lambda = 1.47\ \mu m$ with $P = 15$ W and (**b**) $\lambda = 1.94\ \mu m$ with $P = 5$ W. The arrows mark convective flows. The numbers of radiation rings are marked #1 and #2.

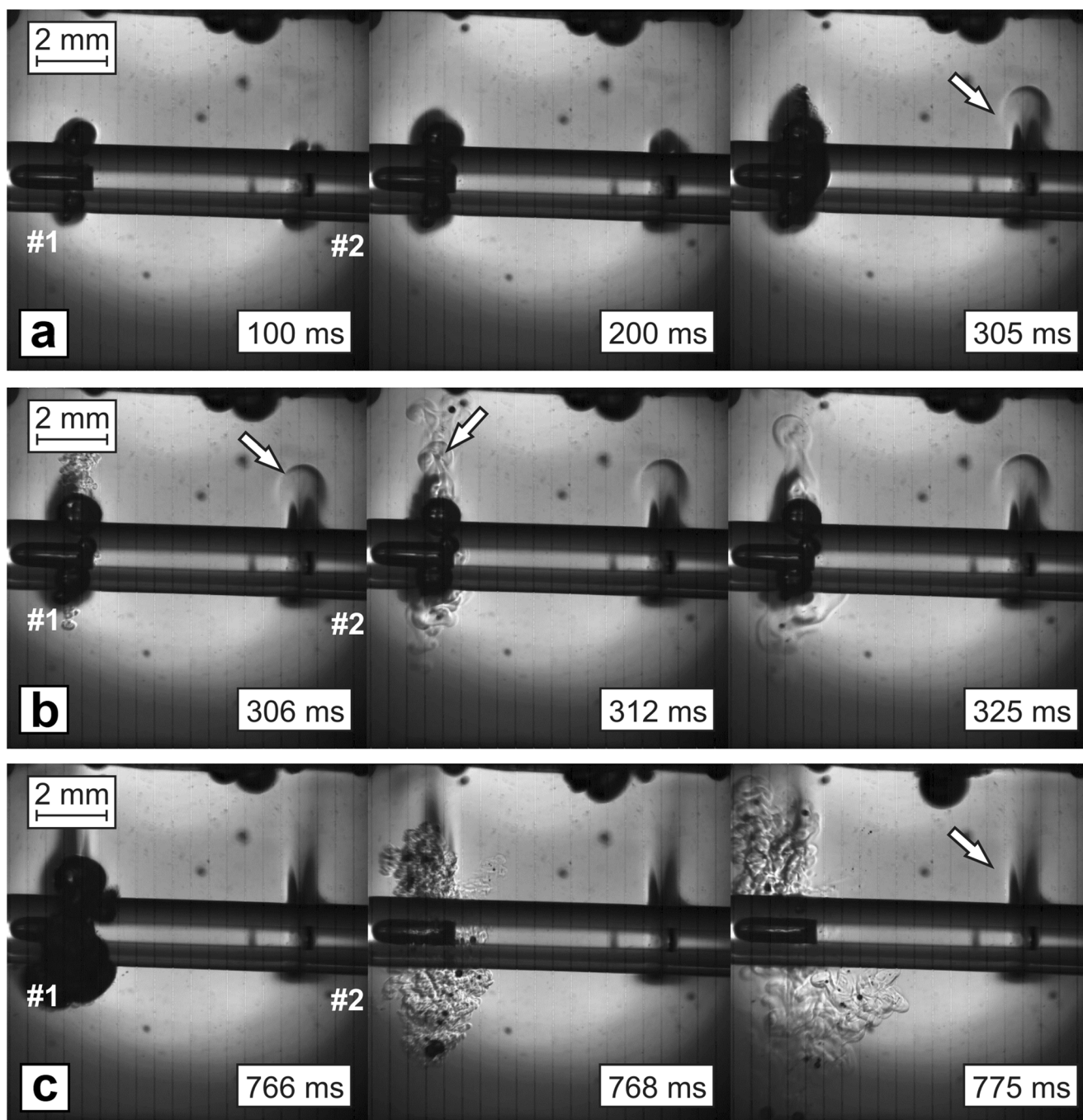**Fig. 7** Dynamics of heat transfer in water when heated by radiation $\lambda = 1.94$ μm with $P = 10$ W through a "two-ring" fiber prior to the explosive boiling. The numbers of radiation rings are marked #1 and #2. The arrow marks convective flow. (**a**) Laser start-up stage. (**b**) The first act of explosive boiling. (**c**) The second act of explosive boiling

heat to the water surrounding them, particularly by forming a vapor gas layer around them. At the same time, local heating of the end of the light guide to high temperature increases sharply, which, when it touch wall, can lead to its perforation and related complications.

Experiments have shown that the dynamics of water heating by continuous laser impact is defined both by the type of fibers (bare-tip, "radial," or "two-ring") and by the radiation wavelengths. The former is obviously connected with different geometry of the radiation output from the fiber, which also determines the density of radiation power, the latter—with the difference in absorption coefficients for laser radiation with different wavelengths in water.

The analysis of shadow patterns shows that in the case of a bare-tip fiber and $\lambda = 1.55$ μm (Fig. 2), heat transfer is initially determined solely by convection. The authors believe that

clear asymmetry in Fig. 2 (temperature gradient is formed near the fiber bottom) is associated with the occurrence of natural convection only at the top of the heated area. The heated and therefore less dense environment is adjacent to a denser one in the bottom part. Therefore, there is no convective mixing.

Experiments have shown that change to radiation with $\lambda = 1.94$ μm (Fig. 3) dramatically changes the pattern of heat transfer: bright pictures of convective heat transfer for $\lambda = 1.55$ μm are absent, and explosive boiling occurs at significantly lower power. Both these changes can be explained by a significantly stronger absorption of laser radiation with $\lambda = 1.94$ μm in water. Strong absorption causes heating of a very thin (h~0.1 mm) layer near the fiber end. In this case, the speed of the convective current will be low due to the proximity of a hard surface, and the overheating that leads to explosive boiling will occur faster and at lower radiation power.

As expected, the replacement of the bare-tip fiber with the "radial" one or with the "two-ring" one significantly changes the heat transfer picture. According to the shadow patterns, the width of rings d (Fig. 1a), through which radiation is emitted from fibers with a protective cap diameter $D = 1.85$ mm can be from 0.23 to 0.32 mm. Appropriate ring aperture areas ($S = \pi \cdot D \cdot d$), through which radiation is emitted, can be estimated from 1.3 to 1.9 mm^2, which by 4.6–6.8 times exceeds the output aperture area of the bare-tip fibers with a diameter of 0.6 mm that equals to 0.28 mm^2.

In the case of the radial fiber, a ring-shaped heated area is formed around the fiber near the radiation output and laminar convection is directed upward (Fig. 4a, b). Thus, gravity prevents a symmetrical transmission of heat relative to the axis.

In the case of "radial" and "two-ring" fiber, the power density at the same laser power is lower due to the significantly larger surface area at the radiation output into water. For the development of the same hydrodynamic processes, their power thresholds increase accordingly. For example, there was no explosive boiling for the radial fiber at $\lambda = 1.55$ μm in the entire range of the studied power (up to 15 W). For $\lambda = 1.94$ μm, they occurred at higher radiation power (Fig. 4b).

The experiments were carried out at room temperature, which is 13 °C lower than body temperature. However, this cannot make noticeable changes in the qualitative picture of the observed processes, since the rates of convective flows are determined by relative heating. As for the observed explosive boiling processes, the increase in the initial temperature will only lead to a slight decrease (according to our estimates, ⁓5%) the heating time required.

To obtain uniform symmetric thermal damage to the vein wall caused by EVLT, it is necessary to use compression of the vein under the influence of tumescent anesthesia until its wall is on the surface of the "radial" or "two-ring" fiber. A more uniform heating of the vein walls can also be ensured by placing it vertically so that the gravity vector is directed along the vein axis.

The authors consider that the results obtained in water qualitatively simulate the processes that occur with the use of bare-tip and "radial" fibers in the clinical application of EVLT for the treatment of varicose veins before the coagulation of organic blood components.

Conclusion

Experimental investigation of heat transfer and hydrodynamic processes during laser heating of water, which to some extent model similar processes occurring during EVLT prior to the coagulation of the organic blood components, have been carried out. The study was conducted in water with various types of optical fibers (bare-tip, "radial," "two-ring") using high-speed surveying of the heating process through the shadow optical method.

It has been shown that in the case of highly water-absorbed laser radiations, convection and boiling play a major role in the process of heat transfer. At the same time, boiling can be small-bubbled (most of the time) or short-term explosive accompanied by the formation of two-phase clouds formed by microbubbles and hot water. This fact shows the inadequacy of mathematical models that consider thermal transfer due to thermal conductivity.

It has been shown that in the case of radiation with $\lambda = 1.94$ μm that is heavily absorbed by water, effective heat transfer begins at significantly lower levels of power compared to the weaker-absorbed radiations with $\lambda = 1.47$ and 1.55 μm. This creates the background for a possible decrease in radiation power that ensures the required EVLT efficiency. In the case of "radial" and "two-ring" fibers, the probability of damaging near the attached cap protecting the distal end of the fiber is much lower.

It has been established that heat transfer is sharply asymmetrical and is directed mainly up-and-forward (bare-tip fiber) or upward ("radial" and "two-ring" fibers). The symmetric heat transfer observed during explosive boiling cannot make a significant contribution because of the short duration of this effect.

Thus, the uniformity of EVLT-induced thermal damage to the vein wall can be achieved only when the vein is compressed under the influence of tumescent anesthesia, until its wall is exposed to the surface of the "radial" or "two-ring" fiber.

References

1. Shimechko OS, Chehovskiy AO, David VM (2014) Comparison of EVLT by lasers with different wavelengths. Materials of the scientific-practical conference "Introduction of modern innovative technologies in minimally invasive laser interventions: clinical, economic and technical aspects" Ukraine. 121–123 [in Ukr.]

2. Cerrati EW, MArch TMO, Chung H, Waner M (2015) Diode laser for the treatment of telangiectasias following hemangioma involution. Otolaryngol - Head Neck Surg (U S) 152:239–243. https://doi.org/10.1177/0194599814559192

3. Mendes-Pinto D, Bastianetto P, Cavalcanti Braga Lyra L et al (2016) Endovenous laser ablation of the great saphenous vein comparing 1920-nm and 1470-nm diode laser. Int Angiol 35:599–604

4. Schmedt C-G, Esipova A, Dikic S et al (2016) Endovenous laser therapy (ELT) of saphenous vein reflux using thulium laser (Tm, 1940 nm) with radial fiber – one year results. Eur J Vasc Endovasc Surg 52:413–414. https://doi.org/10.1016/j.ejvs.2016.07.071

5. Lawson JA, Gauw SA, van Vlijmen CJ et al (2018) Prospective comparative cohort study evaluating incompetent great saphenous vein closure using radiofrequency-powered segmental ablation or 1470-nm endovenous laser ablation with radial-tip fibers (Varico 2 study). J Vasc Surg Venous Lymphat Disord 6:31–40. https://doi.org/10.1016/j.jvsv.2017.06.016

6. Proebstle TM, Lehr HA, Kargl A et al (2002) Endovenous treatment of the greater saphenous vein with a 940-nm diode laser: thrombotic occlusion after endoluminal thermal damage by laser-generated steam bubbles. J Vasc Surg 35:729–736. https://doi.org/10.1067/mva.2002.121132

7. Zhilin KM, Minaev VP, Sokolov AL (2009) Effect of laser radiation absorption in water and blood on the optimal wavelength for endovenous obliteration of varicose veins. Quantum Electron 39:781–784. https://doi.org/10.1070/qe2009v039n08abeh014071

8. Stokbroekx T, De Boer A, Verdaasdonk RM et al (2014) Commonly used fiber tips in endovenous laser ablation (EVLA): an analysis of technical differences. Lasers Med Sci 29:501–507. https://doi.org/10.1007/s10103-013-1475-2

9. Mordon SR, Wassmer B, Zemmouri J (2007) Mathematical modeling of 980-nm and 1320-nm endovenous laser treatment. Lasers Surg Med 39:256–265. https://doi.org/10.1002/lsm.20476

10. Ignatieva NY, Zakharkina OL, Masayshvili CV et al (2017) The role of laser power and pullback velocity in the endovenous laser ablation efficacy: an experimental study. Lasers Med Sci 32:1105–1110. https://doi.org/10.1007/s10103-017-2214-x

11. Poluektova AA, Malskat WSJ, Van Gemert MJC et al (2014) Some controversies in endovenous laser ablation of varicose veins addressed by optical-thermal mathematical modeling. Lasers Med Sci 29:441–452. https://doi.org/10.1007/s10103-013-1450-y

12. Artemov SA, Belyaev AN, Bushukina OS, et al (2019) Optimization of endovenous laser coagulation: in vivo experiments. Lasers Med Sci 9–12. https://doi.org/10.1007/s10103-019-02874-6

13. Artemov S, Belyaev A, Bushukina O, et al (2019) Endovenous laser coagulation using two-micron laser radiation: mathematical modeling and in vivo experiments. In: Book of Abstracts «International Conference on Advanced Laser Technologies (ALT'19)». https://doi.org/10.24411/9999-011A-2019-00154

14. Disselhoff B, Rem AI, Verdaasdonk RM et al (2008) Endovenous laser ablation: an experimental study on the mechanism of action. Phlebology 23:69–76

15. Neumann HAM, Van Gemert MJC (2014) Ins and outs of endovenous laser ablation: afterthoughts. Lasers Med Sci 29:513–518. https://doi.org/10.1007/s10103-013-1499-7

16. Chudnovskii V, Mayor A, Kiselev A, Yusupov V (2018) Foaming of blood in endovenous laser treatment. Lasers Med Sci 33:1821–1826. https://doi.org/10.1007/s10103-018-2552-3

17. Chudnovskii VM, Yusupov VI, Dydykin AV et al (2017) Laser-induced boiling of biological liquids in medical technologies. Quantum Electron 47:361–370. https://doi.org/10.1070/qel16298

18. Minaev VP, Minaev NV, Bogachev VY, et al (2020) Heat transfer in water at laser heating through optic fibers for endovenous laser coagulation. Quantum Electron 50:793-800. https://doi.org/10.1070/QEL17226

19. Marchenko AA, Minaev VP, Smirnov IV, Shevelkina ED (2019) Evaluation of blood optical properties in the wavelength range of 1.3–2.0 μm. Laser Med 23:44–51 (In Russ.)

20. Elhilali MM, Badaan S, Ibrahim A, Andonian S (2017) Use of the Moses technology to improve holmium laser lithotripsy outcomes: a preclinical study. J Endourol 31:598–604